International Journal of Thermophysics, Vol. 27, No. 6, November 2006 (© 2006)
DOI: 10.1007/s10765-006-0122-6

Thermal Diffusivity, Sound Speed, Viscosity, and Surface Tension of R227ea (1,1,1,2,3,3,3-Heptafluoropropane)[1]

A. P. Fröba,[2,3] C. Botero,[2] and A. Leipertz[2]

The purpose of the experimental investigations described in the present paper was to carry out an extensive characterization of R227ea (1,1,1,2,3,3,3-heptafluoropropane), a working fluid that has gained increasing importance in refrigeration and air conditioning technology fields. With dynamic light scattering (DLS), a non-intrusive, laser-optical technique, the thermal diffusivity and sound speed of the liquid and vapor phases, as well as the surface tension and kinematic viscosity of the liquid phase, could be determined with high accuracy at saturation conditions, over a wide temperature range starting at 253.15 K and extending to the critical point.

KEY WORDS: dynamic light scattering; 1,1,1,2,3,3,3-heptafluoropropane; kinematic viscosity; R227ea; sound speed; surface light scattering; surface tension; thermal diffusivity.

1. INTRODUCTION

The fluorinated hydrocarbon R227ea (1,1,1,2,3,3,3-heptafluoropropane) is a long-term alternative in the refrigeration and air conditioning industry to the CFC refrigerants R114 and R12B1, as well as to the CFC refrigerant R12 for certain applications. R227ea is a low-pressure refrigerant and is thus suitable for applications involving high condensation temperatures. The thermodynamic properties of R227ea lie between those of R12 and

[1] Paper presented at the Seventeenth European Conference on Thermophysical Properties, September 5–8, 2005, Bratislava, Slovak Republic.

[2] Lehrstuhl für Technische Thermodynamik (LTT), Friedrich-Alexander-Universität Erlangen-Nürnberg, Am Weichselgarten 8, D-91058 Erlangen, Germany.
[3] To whom correspondence should be addressed. E-mail: apf@ltt.uni-erlangen.de

R114. The volumetric cooling power lies about 50% above that of R114 and 40% below that of R12. The coefficient of performance for the theoretical reference process is smaller than that of refrigerants R12 and R114 [1].

The main application fields of R227ea consist presently of its utilization as a propellant in the production of aerosol sprays in medical technological applications and as a blowing agent in the production of rigid polyurethane foams for insulating purposes. While employed as a pure substance in medical technological applications, R227ea as blowing agent is found as a secondary component in binary mixtures, together with 87 or 93% by mass of R365mfc (1,1,1,3,3-pentafluorobutane) [2,3]. Other areas of application for mixtures of R227ea and R365mfc as the major component are being currently tested. These are thus to be introduced in the future as working fluids in high-temperature heat pumps at condensation temperatures of around 100°C, where high energy savings are achievable through the utilization of the temperature glide of the mixture [4].

In spite of its great technical importance, a lack of data for R227ea can be presently established. This is especially valid for the transport properties, but also for equilibrium data. The major objective of this investigation consists of making a contribution to the improvement and verification of the data situation of R227ea, by means of DLS. In the following, the methodological background of "conventional" DLS for the determination of thermal diffusivity and sound speed will be at first examined, as well as that of surface light scattering (SLS) for the simultaneous determination of kinematic viscosity and surface tension; the experimental conditions will be specified. Subsequently, the results obtained for R227ea will be compared to data available in the literature and discussed.

2. METHOD

The theory presented here for DLS comprises only some fundamental aspects concerning light scattering from the volume of a fluid and from boundary surfaces. A complete and more detailed description of the basic concepts can be found in various fundamental studies [5–12].

2.1. Rayleigh and Brillouin Scattering

The "conventional" DLS is based on an analysis of the Rayleigh and Brillouin light scattering process originating from the volume of a fluid. If a fluid is irradiated with coherent laser light, fluctuating scattered light can be detected in all directions. The underlying scattering process is caused by local statistical fluctuations of the thermodynamic properties

of state pressure and temperature. The compensation process of such statistical fluctuations follows the same laws as those of macroscopic disturbances. Accordingly, temperature fluctuations decrease exponentially with the thermal diffusivity and pressure fluctuations propagate with the speed of sound and are attenuated exponentially with the sound attenuation.

In the light-scattering experiment, the compensation processes mentioned above lead to a temporal modulation of the scattered light, which comprises the information about the dynamics of the molecular motion and thus the substance property data. The analysis of the compensation processes in DLS can be carried out through computation of the time-dependent intensity correlation function $G^{(2)}(\tau)$. For the analysis of temperature fluctuations in a pure fluid under heterodyne conditions, i.e., strong coherent reference light is superimposed to scattered light, this function can be represented by

$$G^{(2)}(\tau) = A + B \exp(-\tau/\tau_{C_t}), \tag{1}$$

where A and B are experimental constants. If the scattering vector q is known, the thermal diffusivity a can be calculated from the correlation time τ_{C_t}, which is identical to the mean lifetime of the contemplated temperature fluctuations, according to

$$a = \frac{1}{\tau_{C_t} q^2}. \tag{2}$$

The value of the scattering vector q is determined by the laser's wavelength in vacuum as well as by the geometry used in the light-scattering experiment; see, e.g., Ref. 8.

For the determination of the sound speed, pressure fluctuations are analyzed. In practice, the frequency ω_S of the contemplated sound waves is established through superposition of scattered light and frequency-shifted reference light. The desired frequency shift $\Delta\omega_M$ is achieved with the aid of an opto-acoustic modulator and is within an order of magnitude of the frequency of the sound waves ($\Delta\omega_M \approx \omega_S$). In this case, the correlation function takes the form,

$$G^{(2)}(\tau) = A + B \exp(-\tau/\tau_{C_B}) \cos(\Delta\omega). \tag{3}$$

The sound speed results from the combination of the known modulation frequency $\Delta\omega_M$ and the residual detuning $\Delta\omega$ of the correlogram according to

$$c_S = \frac{\omega_S}{q} = \frac{\Delta\omega_M \pm \Delta\omega}{q}. \tag{4}$$

2.2. Surface Light Scattering

The method of surface light scattering (SLS) is very similar to that of "conventional" DLS, see Section 2.1. The major difference relies on the fact that, in SLS, fluctuations are analyzed on the surface of a liquid or, in general, on boundary layers between two different phases. Surface waves, whose energy quanta are referred to as "ripplons," form on interfacial boundary layers as a consequence of thermal molecular motion. For the case of low viscosity, as is relevant in the present investigations on R227ea, the amplitude of the surface fluctuations decreases in time as a damped oscillation. In SLS, scattered light emerging from the interaction between light and the fluctuating surface structure is analyzed.

For the completed SLS experiments, the signal analysis was also carried out by computation of the intensity correlation function $G^{(2)}(\tau)$. For light scattered by surface waves under heterodyne conditions, this function can be approximated by

$$G^{(2)}(\tau) = A + B\cos(\omega_R \tau)\exp(-\tau/\tau_{C_R}). \tag{5}$$

Here, the frequency ω_R and the characteristic decay time τ_{C_R} of the correlogram are identical to the frequency and mean decay behavior or attenuation ($\Gamma = 1/\tau_{C_R}$), respectively, of the observed surface fluctuations. As a first approximation, the ratio of the sum of the dynamic viscosities of liquid and vapor to the sum of their densities can be calculated from the decay time τ_{C_R} of the correlogram Eq. (5), for a known scattering vector q, with

$$\frac{\eta' + \eta''}{\rho' + \rho''} \approx \frac{1}{2\tau_{C_R} q^2}. \tag{6}$$

In Eq. (6), η' and η'' denote the dynamic viscosity of the liquid and vapor phases, ρ' and ρ'' their densities. Furthermore, the ratio of the surface tension σ to the sum of the densities of the liquid and vapor phases can be determined from the frequency ω_R of the correlogram, Eq. (5), as a first approximation, through

$$\frac{\sigma}{\rho' + \rho''} \approx \frac{\omega_R^2}{q^3}. \tag{7}$$

An exact description of the relationship involving the dynamic viscosity of the liquid and vapor phases, their densities, and the surface tension with the quantities to be determined in the light scattering experiment, namely, the frequency ω_R, attenuation $\Gamma(=1/\tau_{C_R})$, and wave vector q of the surface waves, is given by their dispersion relation; see, e.g., Refs. 10 and 11.

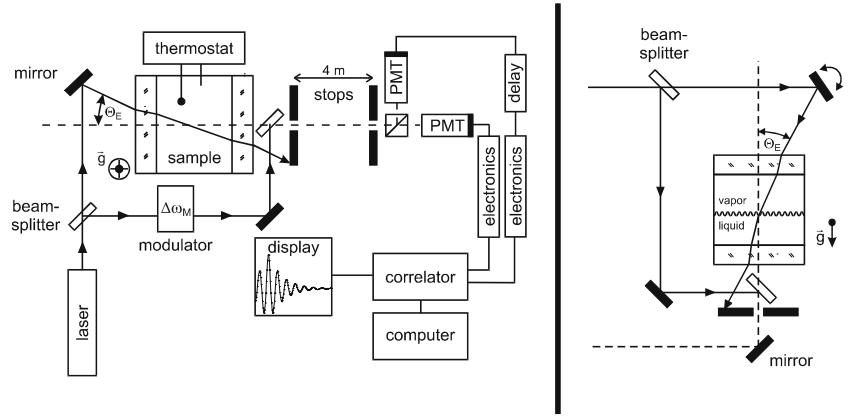

Fig. 1. Experimental setup: optical and electronic arrangement.

The kinematic viscosity of the liquid phase $\nu'(=\eta'/\rho')$ and the surface tension σ were determined, within the scope of this work, by means of an exact numerical solution of the dispersion relation. In addition to the information about the dynamics of the surface fluctuations obtained from the SLS experiment, reference data for the density of both phases and the dynamic viscosity of the vapor phase under saturation conditions were utilized for this purpose.

3. EXPERIMENTAL

The optical and electro-optical components of the experimental setup used for the determination of sound speed and thermal diffusivity are shown—in a top view—on the left side of Fig. 1. For performing light scattering from bulk fluids, the scattering volume, determined by the intersection of the incident beam and the axis of observation (dashed line), is located in the middle of the vessel. The arrangement of the scattering geometry, which enables scattering by surface waves is shown schematically—in a front view—on the right side of Fig. 1. In this case, the optical path has to be aligned in a way that the laser beam and the direction of detection intersect on the liquid–vapor interface in the measurement cell. The basic modification of the setup on the left side of Fig. 1 for carrying out surface light scattering experiments is the mounting of the pressure vessel in a vertical position.

As a light source, an argon ion laser (λ_0 = 488 nm) or optionally a frequency doubled continuous wave Nd:YVO_4 laser (λ_0 = 532 nm) was used. The laser power was as high as 200 mW when working far

away from the critical point, and only a few mW in the critical region. For large scattering intensities, the scattered reference light from the cell windows alone is not sufficient to achieve heterodyne conditions; here, an additional reference beam is added. For this purpose, part of the incident laser light is split by a glass plate and superimposed with the scattered light behind the sample cell. For the determination of the sound speed, a reference beam shifted in frequency by an opto-acoustic modulator was added to the scattered light. The time-dependent intensity of the scattered light is detected by two photomultiplier tubes (PMT's) operated in cross-correlation in order to suppress after-pulsing effects. The signals are amplified, discriminated, and fed to a digital correlator.

With the help of Snell's refraction law and simple trigonometric identities, it can be shown that for both light scattering from bulk fluids and light scattering by surface waves, the scattering vector q can be given as a function of the easily accessible angle of incidence Θ_E, which is defined, see Fig. 1, as the angle between the optical axis of the incident laser beam and the detection direction. In this experiment, the angle of incidence Θ_E was set between 3.0° and 6.0° and was measured with a high-precision rotation table. The errors in the angle measurement have been determined to be approximately ±0.005° and ±0.014° for the observation of light scattered by surface waves and from bulk fluids, respectively. In both cases the error in the angle measurement results in a maximum uncertainty of less than 1% for the desired thermophysical properties.

According to the specifications of the manufacturer (Solvay Fluor GmbH, Hannover), the refrigerant sample had a purity of ≥ 99.9 mass% and was used without further purification. For the present measurements, the sample was filled into an evacuated cylindrical pressure vessel ("conventional" DLS: volume ≈ 10 cm^3; SLS: volume ≈ 150 cm^3) from the liquid phase. The temperature of the pressure vessels, which were placed inside insulated housings, was regulated through resistance heating and measured by calibrated 25-Ω or 100-Ω platinum resistance probes with an uncertainty of ±0.015 K. The temperature stability was better than ±0.002 K during each experimental run. For each temperature point, typically six measurements at different angles of incidence were performed, where the laser was irradiated from either side with respect to the axis of observation in order to check for a possible misalignment. In the SLS experiments, for temperatures below room temperature, the insulating housing was cooled by a lab thermostat to about 10 K below the desired temperature in the sample cell. The measurement times for a single run were typically of the order of 10 min and as small as a few seconds for the highest temperatures in this study. A more detailed description of the experimental setups can be found in Refs. 10 and 12–14.

4. RESULTS AND DISCUSSION

4.1. Thermal Diffusivity and Sound Speed

The data obtained from "conventional" DLS for the thermal diffusivity and sound speed of the refrigerant R227ea in its saturated liquid and vapor phases are shown in Figs. 2 and 3 and are listed in Table I. For each temperature point, the scattering vector q was modified subsequently to give six single measurements, whose mean is presented here. In Figs. 2 and 3, the open symbols represent the measured values for the boiling liquid and the closed symbols those of the saturated vapor. The error bars shown for the liquid phase represent the standard deviation of single measurements, which in "conventional" DLS represents an estimate of the measurement uncertainty [15]. Except for some data near the critical point, overall uncertainties of $\pm 1\%$ for the thermal diffusivity of R227ea and of $\pm 0.5\%$ for the sound speed are estimated. For measurements in the vicinity of the critical point, the standard deviation of both thermal diffusivity and sound speed increased to $\pm 2\%$ and $\pm 1\%$, respectively, which can be attributed to the more difficult experimental accessibility of the critical region.

The continuous curves in Figs. 2 and 3 represent empirical correlations of the experimental data sets. For both phases, the experimental data for the thermal diffusivity as well as for the sound speed can be represented, within the measurement uncertainty, by the sum of a polynomial and an additional term, which accounts for the description of the critical behavior, according to

$$y = \sum_{i=0}^{3} y_i (T/K)^i + \frac{y_4}{(T - T_C^*)/K}. \tag{8}$$

For the boiling and condensation curves, the coefficients of Eq. (8) as well as its range of validity are summarized in Table II. Note that in the data fit according to Eq. (8), T_C^* is not the critical temperature but an additional fit parameter. Also listed in Table II is the root-mean-square deviation of the measured data from Eq. (8), found to be smaller than 0.5% for the sound speed of both phases. The situation appears to be somewhat worse for the thermal diffusivity values, with average standard deviations of 1.21 and 0.63% for the liquid and vapor phases, respectively.

Besides the experimental data sets from DLS, literature data is also included in Figs. 2 and 3 for comparison purposes; the deviations of these data from the regressions of Eq. (8) are displayed in the lower part of the figures. In order to compare the thermal diffusivity values, data calculated by the standard reference database program REFPROP [16] for

Table I. Experimental Values of the Thermal Diffusivity a and Sound Speed c_S of R227ea Under Saturation Conditions

Liquid phase			Vapor phase		
T(K)	a (10^{-8} m^2·s^{-1})	c_S(m·s^{-1})	T(K)	a(10^{-8} m^2·s^{-1})	c_S(m·s^{-1})
293.22	3.66	437.4	345.66	10.14	92.5
303.12	3.50	397.8	348.15	9.30	90.6
313.20	3.26	356.8	350.65	8.46	89.4
323.18	3.14	315.5	353.15	7.64	87.1
332.72	2.95	275.1	355.64	6.90	85.1
342.68	2.76	231.6	358.14	6.06	82.9
348.02	2.66	208.4	360.64	5.25	80.4
353.02	2.51	185.5	363.14	4.41	77.9
358.09	2.36	160.8	365.63	3.60	75.2
363.09	2.11	134.7	367.67	2.91	72.8
365.90	1.92	118.5	369.47	2.26	70.5
368.08	1.72	106.1	370.76	1.78	68.7
370.20	1.42	92.6	371.96	1.32	67.0
371.41	1.21	83.8	372.96	0.921	65.3
372.19	0.991	78.2	373.95	0.490	63.6
372.99	0.788	72.8	374.45	0.265	
373.50	0.611	68.3	374.65	0.173	
373.99	0.434	65.3			
374.49	0.224				
374.67	0.136				

Table II. Coefficients of Eq. (8)

	Thermal diffusivity a y_i (10^{-8} m^2·s^{-1})		Sound speed c_S y_i (m · s^{-1})	
y_i	Liquid phase	Vapor phase	Liquid phase	Vapor phase
y_0	−8.3435	308.5583	1581.25	−1116.73
y_1	0.167719	−1.41054	−3.82084	7.60316
y_2	-66.2154×10^{-5}	159.2760×10^{-5}	-1.3426×10^{-4}	-118.7346×10^{-4}
y_3	7.9231×10^{-7}	–	–	–
y_4	18.843	50.456	1151.37	8.90
T_C^* (K)	380.779	389.118	390.747	377.433
rms (%)	1.21	0.63	0.29	0.11
T-range (K)	293.2 – 374.7	345.7 – 374.7	293.2 – 374.0	345.7 – 374.0

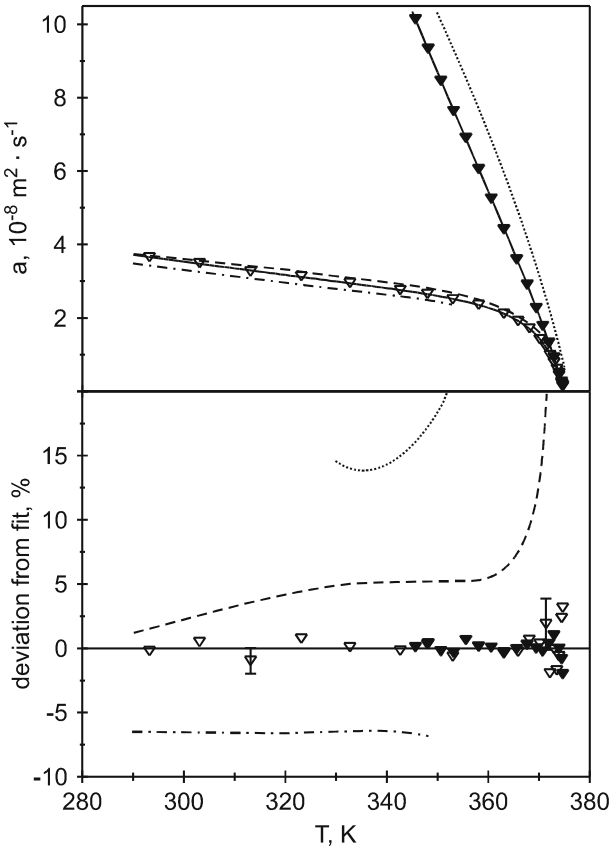

Fig. 2. Data comparison for the thermal diffusivity a of R227ea under saturation conditions: liquid phase, ∇ — this work; - - REFPROP [16]; -·- Baginskii and Stankus [17]; vapor phase, ▼ — this work; ..... REFPROP [16].

both phases, as well as reference data for the thermal conductivity λ of the liquid phase from Baginskii and Stankus [17], are included in Fig. 2. This last data set was converted into thermal diffusivity data a according to $a = \lambda/(\rho c_P)$, with isobaric heat capacity data c_P also originating from the work of Baginskii and Stankus [17], and density values ρ from Ref. 18. Based on a high-frequency temperature wave technique, the thermal-conductivity data from Baginskii and Stankus [17], which were measured for the compressed liquid and subsequently extrapolated to saturation conditions, exhibit deviations of up to 6% with respect to the correlation of the data from DLS. This is found to be within the threshold of the combined

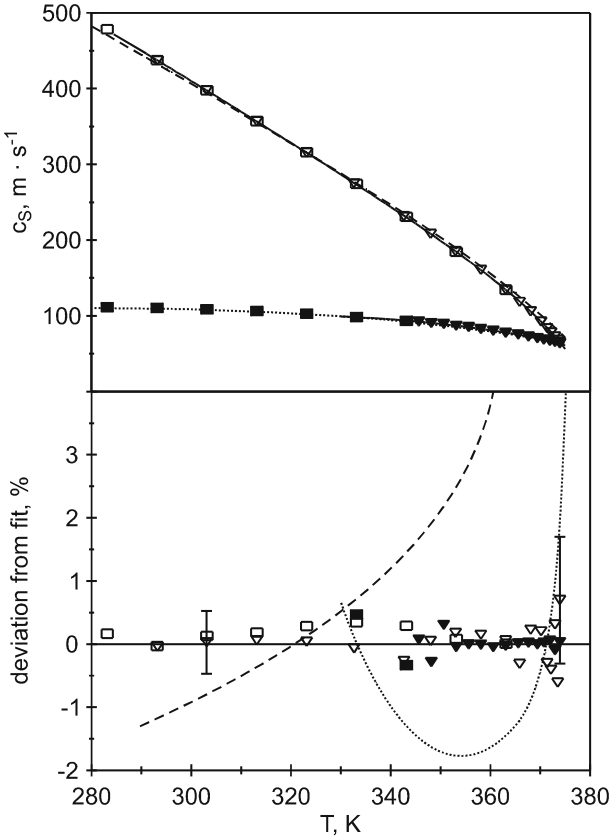

Fig. 3. Data comparison for the sound speed c_S of R227ea under saturation conditions: liquid phase, ▽ — this work; - - REFPROP [16]; □ Gruzdev et al. [19]; vapor phase, ▼ — this work; ..... REFPROP [16], ■ Gruzdev et al. [19].

uncertainty of the diverse measuring techniques, considering the measurement uncertainties of 1.5 and 2% given in Ref. 17 for the thermal conductivity and heat capacity, respectively, as well as the uncertainty associated with the extrapolation of the experimental data sets to saturation conditions. Except in the vicinity of the critical point, the deviations between the data set obtained here and that of the standard reference database program REFPROP [16] were found to be below 5% for the thermal diffusivity of the saturated liquid phase. The saturated-vapor-phase values from REFPROP [16] exhibit positive systematic deviations of more than 50% with respect to the correlation of the experimental data presented here.

For the sound speed in the liquid and vapor phases, Fig. 3 shows the data calculated by the standard reference database program REFPROP [16] as well as those of Gruzdev et al. [19], for comparison purposes. This last set represents measurements along isotherms, extrapolated to saturation conditions, with temperatures ranging from 273 to 393 K and pressures from 0.05 to 35 bar. Measured with an acoustical technique, measurement uncertainties of 0.15–0.2% are specified in Ref. 19 for these sound-speed data. As can be seen from the deviation plot in Fig. 3, Gruzdev's data exhibit very good agreement with the data set obtained from DLS; for example, the sound-speed data obtained here for the liquid deviates by at most 0.35% from those of Gruzdev et al. [19]. Data obtained from the standard reference database program REFPROP [16] show, in contrast, systematic deviations, which become more pronounced when approaching the critical point, reaching levels of more than 5%.

4.2. Kinematic Viscosity and Surface Tension

For the refrigerant R227ea, the results from SLS for the kinematic viscosity of the liquid phase and surface tension at saturation conditions are shown in Figs. 4 and 5, respectively, and listed in Table III. Each data point represents the mean value of typically six independent measurements with different scattering vectors. Besides the results for the kinematic viscosity and surface tension, Table III includes the reference data used for data evaluation, see Section 2.2. The information about the density of the saturated liquid and vapor phases was extracted from Ref. 18. Furthermore, the dynamic viscosity of the saturated vapor phase was calculated theoretically according to a prediction method proposed in Refs. 20 and 21.

Taking into consideration the uncertainties of the individual quantities which were necessary for the data evaluation in the SLS experiments, the overall uncertainty of the kinematic viscosity data of R227ea determined here is estimated to be less than $\pm 1\%$ for the low-temperature region $T/T_C < 0.8$. Even though an increase in the overall uncertainty can be observed with rising temperature, its value does not exceed $\pm 2\%$ as long as the critical point is not approached too closely ($T/T_C < 0.95$). For the simultaneously determined surface-tension data of R227ea, an overall uncertainty of approximately $\pm 1\%$ can be specified. It should be pointed out that a successful determination of both the kinematic viscosity of the liquid phase and surface tension can also be carried out with the use of approximate, or less accurate, values of the dynamic viscosity of the vapor phase. A detailed discussion of the achievable measurement accuracy, when using SLS, can be found in Refs. 10 and 12.

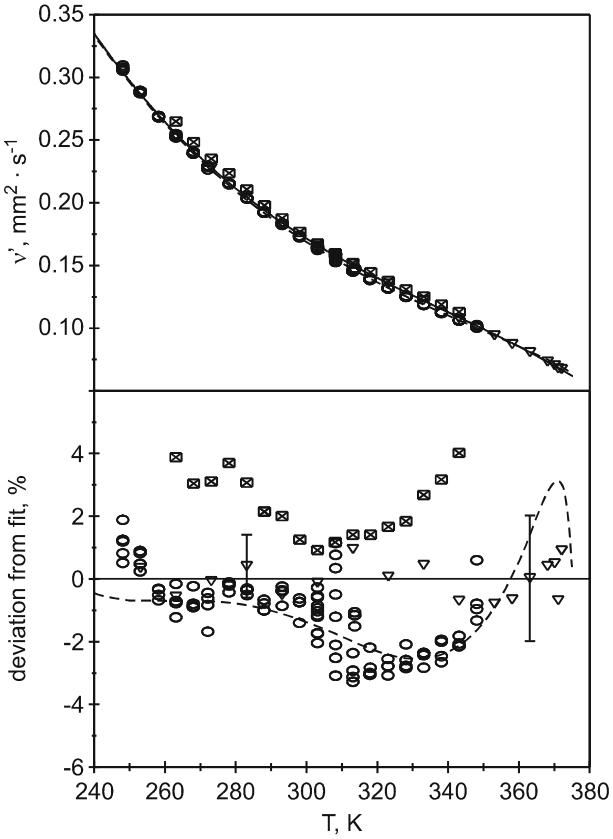

Fig. 4. Data comparison for the kinematic viscosity of the liquid phase ν' of R227ea under saturation conditions: ∇ — this work; - - REFPROP [16]; ⊠ Liu et al. [23]; ◯ Laesecke and Hafer [24].

Even though the temperature dependence of both the dynamic and kinematic viscosities of the saturated liquid phase at a sufficiently large distance from the critical point can be described for many substances by a simple or modified Andrade equation, such a correlation fails to represent the kinematic viscosity data of the refrigerant investigated here up to the vicinity of its critical point. Hence, an empirical description taking the form of a polynomial of third order was chosen;

$$\nu' = \sum_{i=0}^{3} \nu'_i \left(\frac{T}{\mathrm{K}}\right)^i , \tag{9}$$

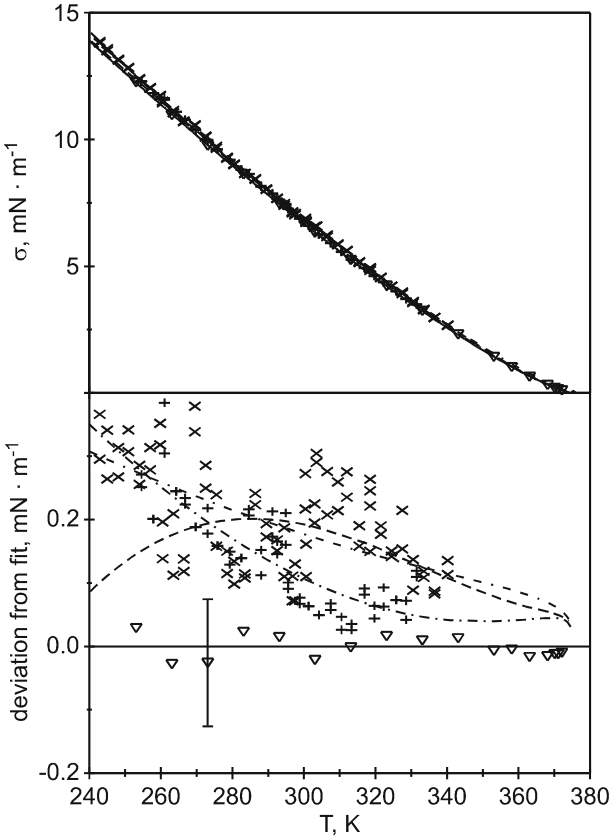

Fig. 5. Data comparison for the surface tension σ of R227ea under saturation conditions: ∇ — this work; - - REFPROP [16]; + -·- Lin and Duan [25]; ×- - · Duan et al. [26].

with which almost every point can be reproduced within the standard deviation of the individual measurements, over the whole temperature range. The coefficients of Eq. (9), obtained from the fit, are listed in Table IV. The root-mean-square deviations of the measurements relative to the values calculated with Eq. (9) are also given in Table IV.

The experimental data for the surface tension can be represented by a modified van der Waals equation, which is suitable for extrapolation of the measurements up to the critical point, according to Ref. 22

$$\sigma = \sigma_0 (1 - T_R)^{1.26} \left[1 + \sigma_1 (1 - T_R)^{0.5} + \sigma_2 (1 - T_R) \right], \tag{10}$$

Table III. Liquid Kinematic Viscosity ν' and Surface Tension σ of R227ea Under Saturation Conditions[a]

T(K)	$\eta''(\mu$Pa·s)	ρ'(kg·m^{-3})	ρ''(kg·m^{-3})	ν'(mm^2·s^{-1})	σ(mN·m^{-1})
253.15	11.2	1557.6	7.3	0.2875	12.26
263.15	11.7	1523.0	11.0	0.2537	10.96
273.15	12.2	1486.6	16.0	0.2278	9.76
283.15	12.7	1448.4	22.6	0.2053	8.62
293.15	13.2	1408.1	31.3	0.1830	7.46
303.15	13.7	1365.4	42.5	0.1659	6.31
313.15	14.3	1319.8	56.8	0.1515	5.25
323.15	15.0	1270.4	75.3	0.1357	4.23
333.15	16.0	1216.0	99.2	0.1224	3.23
343.15	17.3	1154.1	131.0	0.1078	2.30
353.15	18.8	1080.2	175.0	0.0943	1.42
358.15	19.5	1035.6	204.5	0.0874	1.02
363.15	20.4	982.0	242.5	0.0808	0.644
368.15	21.6	911.5	296.0	0.0734	0.314
370.15	22.6	873.9	325.9	0.0703	0.200
371.15	23.4	851.2	344.3	0.0679	0.145
372.15	24.4	824.3	366.3	0.0674	0.097

[a] Directly measured values for frequency ω and damping Γ at a defined wave vector q of surface waves were combined with theoretically calculated data for η'' and literature data for ρ' and ρ'' from Ref. 18 to derive ν' and σ by an exact numerical solution of the dispersion relation.

Table IV. Coefficients of Eq. (9)

ν'_0(mm^2·s^{-1})	4.13024
ν'_1(10^{-2} mm^2·s^{-1})	−3.286066
ν'_2(10^{-5} mm^2·s^{-1})	9.294903
ν'_3(10^{-8} mm^2·s^{-1})	−9.133307
rms (%)	0.56
T-range (K)	253 – 372

where σ_0, σ_1, and σ_2 are the fit parameters listed in Table V. In Eq. (10), $T_R = T/T_C$ represents the reduced temperature, where T is the absolute temperature and T_C is the critical temperature. This last value was obtained by extrapolating the thermal-diffusivity data presented here to zero, which is true at the critical point, estimated to be 374.90 K. This value agrees with the critical temperature of 374.90 K determined experimentally, with an uncertainty of approximately ±0.05 K, with the method of the disappearing meniscus, by observation of the maximum opalescence

Table V. Coefficients of Eq. (10)

σ_0(mN·m^{-1})	52.601
σ_1	−0.0880
σ_2	0.0280
rms (%)	3.51
T-range (K)	253 – T_C

of the sample. The suggested correlation Eq. (10) represents the experimental values of the surface tension with a root-mean-square deviation of approximately 3.5%.

Figure 4 shows a comparison between the data determined with SLS for the kinematic viscosity of liquid R227ea under saturation conditions and those from Liu et al. [23]. Liu et al. [23] estimated an uncertainty of less than 3% in their data, which were obtained with a capillary viscometer. Furthermore, experimental data from Laesecke and Hafer [24] are also compared, originating from capillary viscometers of different types and comprising a measurement uncertainty of ±3.4%, according to Ref. 24. Figure 4 also contains the information provided by the standard reference database program REFPROP [16], which calculates the viscosity of R227ea based on the experimental data from Laesecke and Hafer [24]. Within the combined uncertainties, good agreement of all experimental data sets for R227ea can be established.

Experimental data sets from Lin and Duan [25] and from Duan et al. [26] available in the literature for the surface tension of R227ea, are shown in Fig. 5. Both data sets are based on the differential capillary rise method, with specified measurement uncertainties of approximately ±0.15 mN·m^{-1}. Not only these measurements from Refs. 25 and 26 but also their data correlations are included here, where a simple van der Waals equation is proposed for representing the surface-tension data. Furthermore, Fig. 5 contains the data calculated by the standard reference database program REFPROP [16], which rests on the prediction method given by Schmidt et al. [27]. Within the combined measurement uncertainties, good agreement between the data obtained from SLS and those of Lin and Duan [25] and of Duan et al. [26] can only be found for temperatures above 280 K. In contrast, deviations of the data calculated by the program REFPROP [16] from that of this work are observed to decrease at lower temperatures. Concerning the two data sets coming from Duan's working group [25,26], it should be noted that even between themselves, deviations of up to 0.25 mN·m^{-1} can be observed at low temperatures.

5. CONCLUSIONS

In the context of this work, an extensive characterization of the thermophysical properties of the fluorinated hydrocarbon R227ea was carried out. The thermal diffusivity, sound speed, kinematic viscosity, and surface tension were determined under saturation conditions by means of DLS for a wide temperature range and in the vicinity of the critical point. The overall uncertainties of the thermal diffusivity and sound speed, measured with "conventional" DLS, add up to 1.0 and 0.5%, respectively, except for the data in the vicinity of the critical point. With SLS, the surface tension and kinematic viscosity of the liquid phase could be determined with overall uncertainties of 1.0 and 1.0–2.0%, respectively.

ACKNOWLEDGMENT

The investigated refrigerant has been provided by Solvay Fluor GmbH, Hannover.

REFERENCES

1. H. Buchwald, J. Hellmann, H. König, and C. Meurer, SOLKANE® *Taschenbuch Kälte- und Klimatechnik* (Solvay Fluor & Derivate GmbH, Hannover, 1997).
2. Solvay Fluor & Derivate GmbH, *Solkane® 365/227 Non Flammable Blends – Liquid Foaming Agent for Plastics* (Hannover, 2002).
3. H. Krähling and L. Zipfel, *Proc. Polyurethanes Conf.* (Boston, 2000), pp. 23–31.
4. R. Heidelck, H. Kruse, and H.-J. Laue, *Wärmepumpen in Gewerbe und Industrie – Ein Überblick* (Informationszentrum Wärmepumpen und Kältetechnik e.V., Hannover, 2000).
5. B. J. Berne and R. Pecora, *Dynamic Light Scattering* (Robert E. Krieger, Malabar, 1990).
6. B. Chu, *Laser Light Scattering* (Academic Press, New York, 1991).
7. J. N. Shaumeyer, R. W. Gammon, and J. V. Sengers, in *Measurement of the Transport Properties of Fluids*, W. A. Wakeham, A. Nagashima, and J. V. Sengers, eds. (Blackwell Scientific, Oxford, 1991), pp. 197–213.
8. A. Leipertz and A. P. Fröba, in *Diffusion in Condensed Matter – Methods, Materials, Models,* P. Heitjans and J. Kärger, eds. (Springer, Berlin, 2004), pp. 571–611
9. D. Langevin, *Light Scattering by Liquid Surfaces and Complementary Techniques* (Marcel Dekker, New York, 1992).
10. A. P. Fröba, *Simultane Bestimmung von Viskosität und Oberflächenspannung transparenter Fluide mittels Oberflächenlichtstreuung* (Dr.-Ing. Thesis, Friedrich-Alexander-Universität Erlangen-Nürnberg, Erlangen 2002).
11. E. H. Lucassen-Reynders and J. Lucassen, *Advan. Colloid Interface Sci.* **2**:347 (1969).
12. A. P. Fröba and A. Leipertz, *Int. J. Thermophys.* **24**:895 (2003).
13. A. P. Fröba, S. Will, and A. Leipertz, *Int. J. Thermophys.* **21**:603 (2000).
14. A. P. Fröba, S. Will, and A. Leipertz, *Int. J. Thermophys.* **22**:1021 (2001).
15. K. Kraft, M. M. Lopes, and A. Leipertz, *Int. J. Thermophys.* **16**:423 (1995).
16. *REFPROP Standard Reference Database 23*, Version 7.1 (Nat. Inst. Stds. Technol., Gaithersburg, Maryland, 2003).

17. A. V. Baginskii and S. V. Stankus, *Int. J. Thermophys.* **24**:953 (2003).
18. P. Hu and Z.-S. Chen, *Fluid Phase Equilib.***221**:7 (2004).
19. V. A. Gruzdev, R. A. Khairulin, S. G. Komarov, and S. V. Stankus, *Int. J. Thermophys.* **23**:809 (2002).
20. K. Lucas, *C.I.T.* **46**:157 (1974).
21. R. C. Reid, J. M. Prausnitz, and B. E. Poling, *The Properties of Gases and Liquids* (McGraw-Hill, New York, 1977 and 1987).
22. C. Miqueu, D. Broseta, J. Satherley, B. Mendiboure, J. Lachaise, and A. Graciaa, *Fluid Phase Equilib.* **172**:169 (2000).
23. X.-J. Liu, L. Shi, L.-Z. Han, and M.-S. Zhu, *J. Chem. Eng. Data* **44**:688 (1999).
24. A. Laesecke and R. Hafer, *J. Chem. Eng. Data* **43**:84 (1998).
25. H. Lin and Y.-Y. Duan, *Int. J. Thermophys.* **24**:1495 (2003).
26. Y.-Y. Duan, L. Shi, M.-S. Zhu, L.-Z. Han, and X. Lei, *Fluid Phase Equilib.***172**:273 (2000).
27. J. W. Schmidt, E. Carrillo-Nava, and M. R. Moldover, *Fluid Phase Equilib.***122**:187 (1996).